Petrochemistry of Coal Ash Slags. 2. Correlation of Viscosity with Composition and Petrographic Class

Harold H. Schobert

Grand Forks Energy Research Center
Box 8213, University Station
Grand Forks, ND 58202

The Grand Forks Energy Research Center (GFERC) of the Energy Research and Development Administration has reactivated a fixed-bed slagging coal gasification pilot plant which was formerly operated by the Bureau of Mines. Design of the gasifier, the Bureau of Mines test results, and preliminary results from the ERDA program have been documented (1-4).

A detailed study of the slagging operation is one aspect of the current GFERC pilot plant program. The objective of this study is to develop accurate knowledge of the flow and heat transfer behavior of the slag, both to improve operation of the GFERC plant and to suggest design approaches for future generation gasifiers. One of the important parameters in this work is the slag viscosity.

The experimental determination of slag viscosity as a function of temperature is a difficult procedure. Consequently, many efforts have been made to develop an approach to calculate this relationship. The equations generally proposed incorporate one or more terms which are calculated from the slag composition.

The equation

$$\log_{10}\eta = \frac{10^7 M}{(T-150)^2} + C \qquad [1]$$

has been suggested in several publications (5-7) for calculating viscosity as a function of temperature. In this equation, T is expressed in degrees Centigrade, and η in poises. M and C are terms calculated from the slag composition, being functions of SiO_2, Al_2O_3, Fe_2O_3, and CaO content. Various equations have been proposed for calculating C and M. These equations differ slightly in the values of the coefficients of the composition terms. The work done by Watt and Fereday (6) is based on British coals, while that reported by the Institute of Gas Technology (7) is based on synthetic melts.

Attempts were made to use equation [1] for the calculation of viscosities of some lignite ash slags for which experimental viscosity data was available at GFERC. Both the Watt-Fereday method (5,6) and the modified equations suggested by Bomkamp (7) were used. A test temperature was selected from the center of the temperature range over which viscosity data was available at GFERC (8). Some of the results are given in Table 1.

TABLE 1. Calculated Values of Lignite Slag Viscosities.[A/]

Lignite Slag	Temperature	Method 1[B/]	Method 2[C/]	Expt'l Value
Baukol-Noonan	1175°	197	11,600	42
Indianhead	1260°	21	2,276	60
Velva	1385°	<1	1	350

A/ Sources and compositions of the coal ash slags are given in the appendix.

B/ Watt-Fereday Method. C/ Modified Watt-Fereday Method.

Since the results shown in Table 1 are clearly unsatisfactory, the development of additional modifications to equation [1] was undertaken. Since the GFERC gasification program will test a variety of Western lignite and subbituminous coals, it was desired to develop an equation applicable to the widest possible range of slag compositions. Viscosity-temperature data were available for slags having the range of compositions shown below.

TABLE 2. Range of Slag Compositions Used in GFERC Study

Component	Range, Pct	Component	Range, Pct
SiO_2	15-49	MgO	1-10
Al_2O_3	9-27	Na_2O	.3-12
Fe_2O_3	7-23	K_2O	.1-4
CaO	3-43		

Equation [1] was rewritten as

$$Y = MX + C$$

where $X = 10^7/(T-150)^2$ and $Y = \log_{10}\eta$. The experimental data were then used to compute values of M and C for each slag, using a standard linear regression computer program. The results are given in Table 3.

TABLE 3. Values of C and M Computed by Linear Regression

Slag[A/]	C	M
Baukol-Noonan	-1.2180	.3069
Bentinck	- .8604	.5851
Cronton-19[B/]	-1.2194	.5288
Cronton-27[C/]	- .9997	.5849
Dickinson	-4.1015	.5945
Disco	- .5266	.4240
Disco-Flux[D/]	- .8429	.2948
Indianhead	-4.0781	.7264
Thoresby	- .7840	.4892
Velva	-7.2934	1.4996

A/ Source and composition data is given in the appendix.
B/ 19 pct ash coal. C/ 27 pct ash coal.
D/ 3 lb. blast furnace slag added per lb. of ash.

The computed values of C and M were used as input data for a multiple linear regression analysis for the development of equations relating C and M to slag composition. Repeated computer trials failed to produce a satisfactory fit of the data. As a result, attention was then focused on performing regression analyses for slags only of a single petrographic class. (In this paper petrographic classifications and terminology refer to igneous rock petrography, rather than to coal petrography.)

The test slags were divided into two groups on the basis of similarity of composition: Baukol-Noonan, Disco-Flux, and Indianhead in the first group; and Bentinck, Cronton-19, Cronton-27, Disco, and Thoresby in the second. Detailed petrographic analyses were done for Indianhead and Thoresby slags, the compositions of which are given in the appendix. The petrographic classification was done by the C.I.P.W. method (9), following the procedure outlined by Johannsen (10). This procedure is a taxonomic method for comparing chemical analyses from a petrological aspect. The analytical data is recalculated in terms of a set of standard mineral molecules. Indianhead slag was found to be pyroxene normative and Thoresby to be feldspar normative.

Correlation coefficients were calculated between each of the major slag components and the values of C and M, for both classes of slag. The calculations were done using a standard linear correlation computer program. This work was done so that the results would serve as a guide to which slag components might best be used in a multiple regression analysis for developing equations to calculate C and M. The computed values of the correlation coefficients are given in Table 4.

TABLE 4. Linear Correlation Coefficients Between Slag Composition and Computed Values of C and M.

	Pyroxene-normative Slags		Feldspar-normative Slags	
Component	C	M	C	M
SiO_2	-.369	.444	.681	.094
Al_2O_3	.554	-.485	-.573	.570
Fe_2O_3	-.996	.999	-.019	-.512
CaO	.360	-.283	.168	.255
MgO	.209	-.129	-.495	.200
Na_2O	-.140	.059	.030	.140
K_2O	-.589	.521	-.760	.940

Multiple linear regression analysis of the feldspar normative group developed the following equations:

$$C = -4.5413 - .2158\ (K_2O) + .0883\ (SiO_2) + .0091\ (Al_2O_3) \qquad [3]$$

$$M = 0.3676 + .0783\ (K_2O) - .0043\ (Al_2O_3) \qquad [4]$$

In these equations the concentration terms use the actual weight percent values determined from the chemical analysis.

The viscosity-temperature relationship for Cronton-19 slag was calculated by substituting equations [3] and [4] into equation [1]. The appropriate analytical data for this slag are 3.5 pct K_2O, 43.6 pct SiO_2, and 24.6 pct Al_2O_3. Figure 1 shows the experimental (11) and calculated viscosity curves.

Although only limited data are available for the pyroxene normative slags, a regression analysis was done to fit C and M values to Fe_2O_3 content because of the high correlation between these parameters. Equations [5] and [6] resulted.

$$C = 0.8143\ (Fe_2O_3) - 4.8749 \qquad [5]$$

$$M = 0.1135\ (Fe_2O_3) - .5219 \qquad [6]$$

The viscosity-temperature curve for Indianhead slag (Fe_2O_3 = 11.0 pct) calculated from equations [5], [6], and [1], is given in Figure 2.

These results demonstrate that this approach produces improved results for the specific slags studied thus far. It is suggested that classification of slags by a petrographic procedure may be more useful than other methods for the production of viscosity effects.

REFERENCES

1. G.H. Gronhovd, A.E. Harak, W.R. Kube, and W.H. Oppelt. "Design and Initial Operation of a Slagging, Fixed-Bed, Pressure Gasification Pilot Plant." U.S. Bureau of Mines RI 6084 (1962).

2. G.H. Gronhovd, A.E. Harak, M.M. Fegley, and D.E. Severson. "Slagging Fixed-Bed Gasification of North Dakota Lignite at Pressures to 400 Psig." U.S. Bureau of Mines RI 7408 (1970).

3. R.C. Ellman and B.C. Johnson. "Slagging Fixed-Bed Gasification at the Grand Forks Energy Research Center." Presented at the Eighth Synthetic Pipeline Gas Symposium, Chicago, IL, October 1976.

4. R.C. Ellman and H.H. Schobert. "Pilot Plant Operation of a Fixed-Bed Slagging Gasifier." Presented at the National Meeting of the American Chemical Society, New Orleans, LA, March 1977.

5. British Coal Utilization Research Association, Annual Report (1963).

6. J.D. Watt and F. Fereday. "The Flow Properties of Slags Formed from the Ashes of British Coals: Part 1: Viscosity of Homogeneous Liquid Slags in Relation to Slag Composition." J. Inst. Fuel, 42, 99 (1969).

7. Institute of Gas Technology. "Preparation of a Coal Conversion Systems Technical Data Book." Energy Research and Development Administration Report FE-1730-21 (1976).

8. G.H. Gronhovd. Private communication.

9. H.S. Washington. "Chemical Analyses of Igneous Rocks." U.S. Geological Survey Professional Paper 99 (1917).

10. A. Johansen. "A Descriptive Petrography of Igneous Rocks." The University of Chicago Press, Chicago, IL (1939).

11. H.R. Hoy, A.G. Roberts, and D.M. Wilkins. "Some Investigations with a Small Cyclone Combustor." J. Inst. Fuel, 31, 441 (1958).

APPENDIX

Composition and Source Data for Slags Used in this Study

Slag:	Baukol-Noonan	Bentinck	Cronton-19	Cronton-27	Dickinson	Disco	Disco & Flux	Indian-head	Thorseby	Velva
Source:	North Dakota	British	British	British	North Dakota	Pennsyl-vania	A/	North Dakota	British	North Dakota
Rank:	Lignite	Bituminous	Bituminous	Bituminous	Lignite	Bituminous		Lignite	Bituminous	Lignite
Slag Analysis, wt. %	B/	C/	C/	C/	B/	B/	B/	B/	C/	B/
SiO_2	33.0	48.9	43.6	47.7	21.8	48.0	39.8	39.5	46.7	14.7
Al_2O_3	13.5	23.2	24.6	27.1	9.1	23.0	15.6	13.6	23.4	11.1
Fe_2O_3	7.3	6.6	17.4	11.8	23.1	18.5	7.2	11.0	6.9	6.7
CaO	14.5	10.5	3.5	2.7	18.4	3.3	27.2	17.9	8.4	43.3
MgO	4.4	1.6	2.3	1.9	7.2	1.0	6.6	5.3	2.9	10.1
Na_2O	12.1	1.7	0.8	0.5	0.6	0.3	0.4	6.6	2.4	4.4
K_2O	1.0	3.5	3.4	4.2	0.1	1.9	0.5	1.0	3.0	0.3

A/ Disco ash fluxed with 3 lb. blast furnace slag per lb. of ash.
B/ GFERC data.
C/ Data of Hoy, Roberts & Wilkins (11).

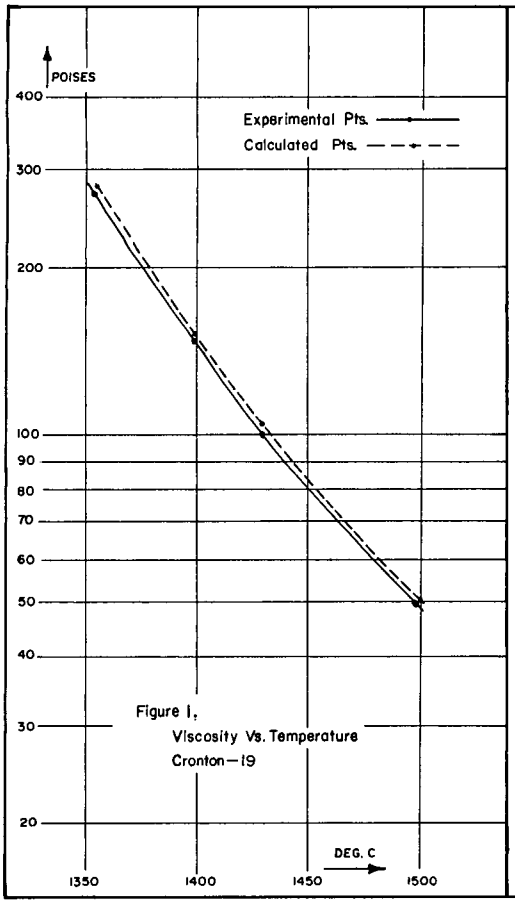

Figure 1.
Viscosity Vs. Temperature
Cronton—19

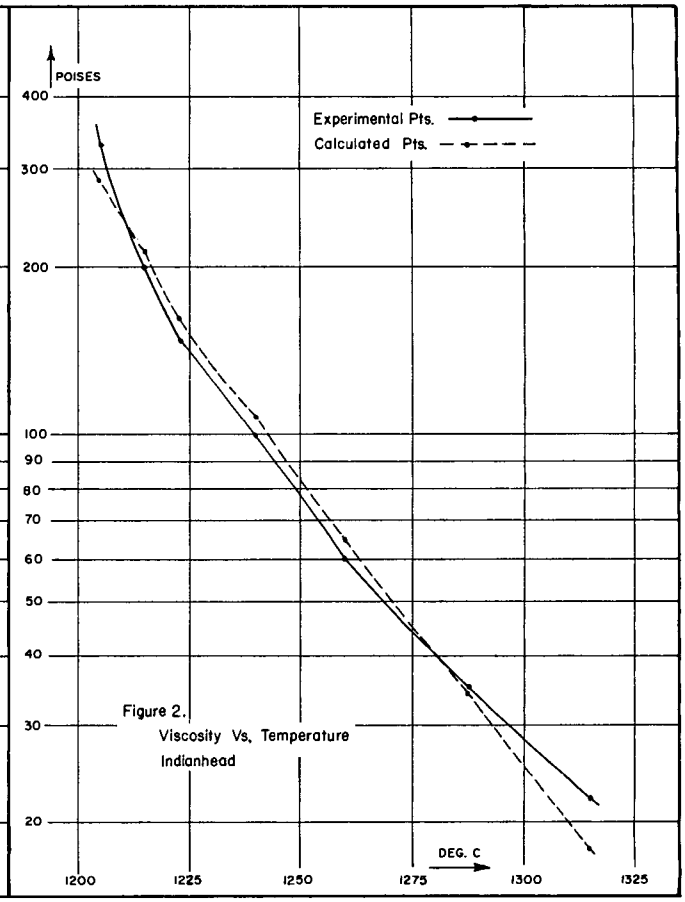

Figure 2.
Viscosity Vs. Temperature
Indianhead

SIZE-DEPENDENCE OF THE PHYSICAL AND CHEMICAL PROPERTIES OF COAL FLY ASH*

G. L. Fisher,[1] B. A. Prentice,[1] D. Silberman,[1] J. M. Ondov,[2]
R. C. Ragaini,[2] A. H. Bierman,[2] A. R. McFarland,[3] and J. B. Pawley.[4]

[1]Radiobiology Laboratory, University of California, Davis, CA 95616
[2]Lawrence Livermore Laboratory, Livermore, CA 94550
[3]Civil Engineering Department, Texas A & M University, College Station, TX 77843
[4]Donner Laboratory, University of California, Berkeley, CA 94720

In order to aid in the assessment of the potential biomedical and environmental consequences of coal combustion for electric power generation, we have performed detailed collaborative studies of the physical and chemical properties of size-fractionated coal fly ash. In this report, we demonstrate that many of the physical and chemical properties of aerodynamically size-classified fly ash depend on the relative size distributions of each fraction.

Aerodynamically size-classified fly ash was collected downstream from the electrostatic precipitator (ESP) in the stack breeching of a large southwestern U. S. power plant burning low sulfur (0.5%), high ash (23%) coal. The specially designed collection system (1) which consists of two cyclones and a centripeter separator is capable of size-classifying *in situ* kilogram quantities of stack fly ash. When used for 12 days to collect fly ash from stack gas, the apparatus yielded a total of 8.08 kg of fly ash in fractions with volume median diameters (VMD) of 20 μm (fraction 1), 6.3 μm (fraction 2), 3.2 μm (fraction 3) and 2.2 μm (fraction 4) all with geometric standard deviations of approximately 1.8. The size distribution data determined by optical sizing, centrifugal sedimentation and Coulter analyses are presented in Table 1.

Physical Studies

Based on light microscopic study of the four fly ash fractions, we have developed a particle morphogenesis scheme (Fig. 1). The physical characteristics of opacity, shape and type of inclusion utilized in the morphogenesis scheme appear to be related to degree and extent of exposure of the fly ash to combustion zone temperatures.

Eleven particle types and their probable matrix composition are classified (Fig. 1): 1) amorphous, non-opaque, 2) amorphous, opaque, 3) amorphous, mixed opaque and non-opaque, 4) rounded, vesicular, non-opaque, 5) rounded, vesicular, mixed opaque and non-opaque, 6) angular, lacy, opaque, 7) non-opaque, cenosphere (hollow sphere), 8) non-opaque, plerosphere (sphere packed with other spheres), 9) non-opaque, solid sphere, 10) opaque sphere and 11) non-opaque spheres with either surface or internal crystals. We have quantified the relative abundances of each of the 11 morphologic particle types in the four fractions (Table 2). The relative abundance of all particle types except non-opaque, solid spheres appears to increase with the increasing particle size of the fly ash fractions. The relative abundance of non-opaque, solid spheres is inversely dependent on particle size. Chi-square analyses of the relative distribution data of the morphologic particle types in the four fly ash fractions indicated highly significant ($p < 0.001$) differences for all six possible comparisons.

The apparent densities of the four fractions (Table 2) can be negatively correlated ($r = -0.978$; $p < 0.05$) with the VMD's. Furthermore, linear regression analyses of the fractional distribution data with the densities of the individual size fractions indicate significant ($p < 0.05$) positive correlations for the following particle types: 1) amorphous, non-opaque, 4) rounded, vesicular, non-opaque, 7) non-opaque cenospheres and 10) opaque sphere. Significant negative correlation was found only for solid, non-opaque spheres ($p < 0.01$).

*This work was supported by the US Energy Research and Development Administration.

Chemical Studies

The fly ash fractions were analyzed for 35 elements by instrumental neutron activation analysis (INAA) at the Lawrence Livermore Laboratory and for 18 elements by atomic absorption spectroscopy (AAS) at the Radiobiology Laboratory. The analytical techniques have been previously described (2). Before analyses of the fly ash fractions were undertaken both laboratories performed analyses of the National Bureau of Standards (NBS) Standard Reference Material, Trace Elements in Coal Fly Ash (SRM 1633). Agreement of all analytical results from both laboratories with previously published (3) or NBS certified values was excellent. The interlaboratory comparison has been reported by Ondov *et al.* (2).

Summary tables of the analytical results are presented for those elements displaying concentrations independent of particle size (Table 3) and dependent on particle size (Table 4). For elements analyzed by both INAA and AAS, the data reported are the results of the analytical technique with the smaller coefficient of variation. Data from atomic absorption analyses are the average of two independent determinations; the INAA data are the weighted averages of three independent determinations. Concentration dependence with particle size was determined qualitatively with the criteria that consistent concentration trends beyond experimental uncertainty were observed for each fraction, although significantly higher concentrations of the element may have been observed in the finest fraction relative to the coarsest fraction.

With the exception of silicon, which appears to decrease with decreasing particle size, the major element composition of the fractionated fly ash is relatively independent of particle size. Greater than 92% of the mass of the fractionated fly ash can be accounted for by oxides of Si, Al, Fe and Ca. An enhancement factor was defined as the ratio of the element concentration in cut 4 (finest) to its concentration in cut 1 (coarsest). The more volatile elements (or their oxides), Cd, Zn, Se, As, Sb, Mo, Ga, Pb and V display clear-cut increases in concentration with decreasing particle size, in agreement with the vapor-condensation mechanism of Natusch and Wallace (4). It is important to note, however, that refractory elements also display concentration trends inversely dependent on particle size. Therefore, processes other than vapor condensation are involved in the concentration-size relationship. The elements U and Cr are associated with the organic fraction of coal (5) and may be released in the combustion process as fine particles which may agglomerate with other particles. The elements Fe, Mn, Ba, and Sr (5) may in part be present as carbonate minerals which decompose to form fine particles during coal combustion and again agglomerate with other particles. Copper is probably present in part as the sulfide and Be as the aluminosilicate in the coal (5). Thus, mineral decomposition and elemental distribution may in part explain the elemental trends of the high boiling chemical species.

In summary, many physical and chemical properties of coal fly ash are dependent on particle size. Apparent density varies inversely with particle size and may be explained by the higher relative abundance of vesicular particles and lower relative abundance of solid, non-opaque spheres in larger size fractions. The elements Al, Fe, Ca, Na, K, Ti, Mg, Sr, Ce, La, Rb, Nd, Th, Ni, Sc, Hf, Co, Sm, Dy, Yb, Cs, Ta, Eu and Tb do not display clear-cut concentration trends with particle size. Silicon was the only element analyzed with clear-cut direct concentration dependence with particle size. Inverse concentration dependence with particle size was observed for Cd, Zn, Se, As, Sb, W, Mo, Ga, Pb, V, U, Cr, Ba, Cu, Be and Mn. Although a vapor-condensation mechanism may explain the concentration trends for the volatile elements, mineral decomposition and elemental distribution within the coal are probably important processes contributing to the inverse concentration dependence observed for the higher boiling chemical species.

References

1. McFarland, A. R., Fisher, G. L., Prentice, B. A., Bertch, R. W. Submitted to Environ. Sci. Technol.

2. Ondov, J. M., Ragaini, R. C., Heft, R. E., Fisher, G. L., Silberman, D., Prentice, B. A. Proc. NBS 8th Materials Research Symposium, Gaithersburg, MD. September, 1976, in press.

3. Ondov, J. M., Zoller, W. H., Omez, I., Aras, N. K., Gordon, G. E., Rancitelli, L. A., Abel, K. H., Filby, R. H., Shah, K. R., Ragaini, R. C. Anal. Chem. 47, 1102 (1975).

4. Natusch, D. F. S., Wallace, J. R. Science 186, 695 (1974).

5. Murchison, D., Westoll, T. S. "Coal and coal-bearing strata", 418 pp, American Elsevier, N. Y., 1968.

Table 1. Size Parameters for the Fly Ash Fractions

Fraction	CMD[1]		MMD[2]		VMD[3]	
	μm	σg[4]	μm	σg	μm	σg
1	2.73	2.20	18.5	2.8	20.0	1.8
2	2.58	1.86	6.0	2.0	6.3	1.8
3	1.14	1.73	3.7	1.7	3.2	1.8
4	0.92	1.52	2.4	1.8	2.2	1.9

[1]Count median diameter determined from scanning electron micrographs.
[2]Mass median diameter determined from Stokes differential settling in aqueous dispersion.
[3]Volume median diameter determined by Coulter analysis.
[4]Geometric standard deviation.

Table 2. Relative Abundance (%) of Morphologic Particle Types in the Four Fly Ash Fractions[1]

	Particle Type	Fraction 1	2	3	4
1.	Amorphous, non-opaque	7.25	2.13	0.79	0.33
2.	Amorphous, opaque	0.42	0.18	--	--
3.	Amorphous, mixed opaque and non-opaque	0.77	0.09	--	--
4.	Rounded, vesicular, non-opaque	12.39	6.67	2.91	2.99
5.	Rounded, vesicular, mixed opaque and non-opaque	2.27	0.24	--	0.03
6.	Angular, lacy, opaque	1.34	0.57	0.27	0.33
7.	Non-opaque, cenosphere	41.11	26.22	13.20	7.91
8.	Non-opaque, plerosphere	0.51	0.21	--	--
9.	Non-opaque, solid sphere	25.58	56.01	79.16	86.99
10.	Opaque sphere	1.56	0.90	0.33	0.24
11.	Non-opaque sphere with crystals	6.80	6.79	3.18	0.95
12.	Combined[2] particle types 2 and 6	--	--	0.15	0.24
	VMD (μm)	20	6.3	3.2	2.2
	Density[3] (g/cm^3)	1.85	2.19	2.36	2.45

[1]A total of approximately 3000 particles for each size fraction were classified from random fields using three microscope slides per fraction.
[2]Combined due to inability to distinguish between these classes for the finer particles.
[3]Apparent density determined by gravimetric displacement of 1-propanol.

Table 3. Elemental Concentrations Independent[1] of Particle Size

Element	Technique	Fraction 1 (VMD = 20 μm)	Fraction 2 (VMD = 6.3 μm)	Fraction 3 (VMD = 3.2 μm)	Fraction 4 (VMD = 2.2 μm)
		Concentration in %			
Al	AAS[2]	13.8(0.1)	14.4(0.1)	14.2(0.8)	14.1(0.3)
Fe	INAA[3]	2.5(0.1)	2.9(0.2)	3.0(0.1)	3.2(0.1)
Ca	AAS	2.12(0.14)	2.23((0.08)	2.30(0.14)	2.38(0.09)
Na	AAS	1.19(0.13)	1.75(0.05)	1.83(0.06)	1.85(0.03)
K	AAS	0.74(0.01)	0.80(0.07)	0.82(0.08)	0.81(0.03)
Ti	AAS	0.62(0.05)	0.76(0.05)	0.77(0.11)	0.78(0.06)
Mg	AAS	0.47(0.01)	0.56(0.01)	0.60(0.02)	0.63(0.01)
		Concentration in μg/g			
Sr	INAA	410(60)	540(140)	590(140)	700(210)
Ce	INAA	113(4)	122(5)	123(6)	120(5)
La	INAA	62(3)	68(4)	67(11)	69(3)
Rb	INAA	51(3)	56(4)	57(3)	57(8)
Nd	INAA	45(4)	47(4)	49(7)	52(6)
Th	INAA	25.8(0.6)	28.3(0.6)	29(1)	30(2)
Ni	AAS	25(3)	37(1)	43(4)	40(2)
Sc	INAA	12.6(0.5)	15.3(0.6)	15.8(0.6)	16.0(0.2)
Hf	INAA	9.7(0.4)	10.3(0.3)	10.5(0.3)	10.3(0.5)
Co	INAA	8.9(0.2)	16.3(0.8)	19(1)	21(1)
Sm	INAA	8.2(0.3)	9.1(0.4)	9.2(0.4)	9.7(0.4)
Dy	INAA	6.9(0.3)	8.5(0.9)	8.1(0.3)	8.5(0.8)
Yb	INAA	3.4(0.4)	4.1(0.4)	4.0(0.2)	4.2(0.3)
Cs	INAA	3.2(0.1)	3.7(0.2)	3.7(0.2)	3.7(0.2)
Ta	INAA	2.1(0.1)	2.3(0.2)	2.5(0.3)	2.7(0.1)
Eu	INAA	1.0(0.1)	1.2(0.2)	1.2(0.2)	1.3(0.4)
Tb	INAA	0.90(0.05)	1.06(0.06)	1.10(0.07)	1.13(0.06)

[1]Concentration dependence with particle size was determined qualitatively with the criteria that consistent concentration trends beyond experimental uncertainty were observed for each fraction.

[2]AAS values are the averages of two independent determinations; the ranges are given in parentheses.

[3]INAA values are the weighted averages of three independent determinations; uncertainties (in parentheses) are the largest of twice the weighted standard deviation, the range, or an estimate of the accuracy.

Table 4. Elemental Concentrations Dependent[1] on Particle Size

Element	Technique	Fraction 1 (VMD = 20 μm)	Fraction 2 (VMD = 6.3 μm)	Fraction 3 (VMD = 3.2 μm)	Fraction 4 (VMD = 2.2 μm)	Enhancement Factor[2]
		Concentration in μg/g (unless indicated)				
Cd	AAS[3]	0.4(0.2)	1.6(0.3)	2.8(0.4)	4.6(0.2)	11.5
Zn	AAS	68(1)	189(4)	301(10)	746(218)	11.
Se	INAA[4]	19(2)	59(2)	78(2)	198(20)	10.4
As	INAA	13.7(1.3)	56(14)	87(9)	132(22)	9.6
Sb	INAA	2.6(0.1)	8.3(0.4)	13.0(0.7)	20.6(0.7)	7.9
W	INAA	3.4(0.2)	8.6(1.6)	16(2)	24(2)	7.1
Mo	INAA	9.1(2.5)	28(1.4)	40(5)	50(9)	5.5
Ga	INAA	43(12)	116(52)	140(23)	178(90)	4.1
Pb	AAS	73(3)	169(2)	226(4)	278(3)	3.8
V	INAA	86(44)	178(17)	244(18)	327(40)	3.8
U	INAA	8.8(1.9)	16(3)	22(4)	29(4)	3.3
Cr	AAS	28(3)	54(3)	66(3)	71(4)	2.5
Ba(%)	AAS	0.168(0.001)	0.245(0.002)	0.320(0.013)	0.409(0.018)	2.4
Cu	AAS	56(1)	89(1)	107(4)	137(1)	2.4
Be	AAS	6.3(0.2)	8.5(0.2)	9.5(0.3)	10.3(0.5)	1.6
Mn	AAS	209(7)	231(5)	273(7)	309(3)	1.5
Si(%)	AAS	29.6(0.7)	28.0(0.1)	27.5(0.3)	26.8(0.1)	0.90

[1]Concentration dependence with particle size was determined qualitatively with the criteria that consistent concentration trends beyond experimental uncertainty were observed for each fraction.
[2]Ratio of concentration in Fraction 4 to that in Fraction 1.
[3]AAS values are the averages of two independent determinations; the ranges are given in parentheses.
[4]INAA values are the weighted averages of three independent determinations; uncertainties (in parentheses) are the largest of twice the weighted standard deviation, the range, or an estimate of the accuracy.

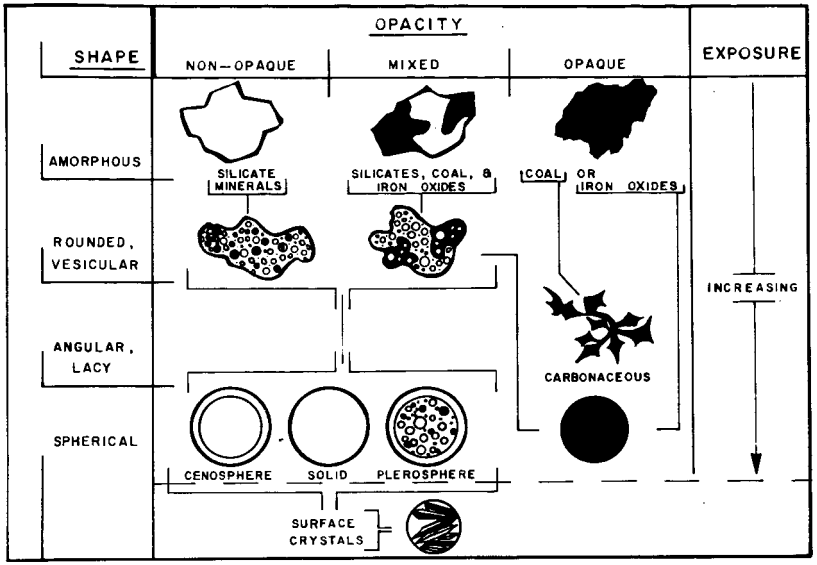

Fig. 1. Fly ash morphogenesis scheme illustrating probable relationship of opacity and shape to particle composition and exposure in the combustion chamber.

NOT FOR PUBLICATION
For Presentation Before the Division of Fuel Chemistry
American Chemical Society
Montreal, Quebec, Canada, May 1977

THE BEHAVIOR OF THE NATURAL RADIONUCLIDES IN WESTERN COAL-FIRED POWER PLANTS

David G. Coles, Richard C. Ragaini, and John M. Ondov

Division of Environmental Research, Lawrence Livermore
Laboratory, University of California, Livermore, CA 94550

The projected dependence of the nation on coal-produced electrical energy necessitates a thorough study of the associated environmental risks. One potential hazard worthy of further investigation is the release of natural radionuclides upon coal combustion. Radioactive effluents from both fossil-fuel and nuclear power plants have been compared.[1,2] However, oversimplifications and lack of good emission data for radionuclides from the fossil-fuel plants lead to differing conclusions. Hull[3] has compared the inorganic-effluent releases of the fossil-fuel plants to the radionuclide releases from nuclear plants in terms of accepted environmental standards for each type of effluent. Moore et al.[4] have calculated that anthropogenic sources contribute 6.5% of the total ^{210}Po atmospheric flux for the continental U.S. Fossil-fuel burning makes up 14% of these anthropogenic sources or 1% of the total ^{210}Po input. One can determine a maximum concentration indirectly from the ^{210}Pb content in the coal, since ^{210}Pb is the grandparent of ^{210}Po in the ^{238}U-decay series. None of the fossil-fuel-plant studies have concentrated on the radionuclide-combustion chemistry, which is necessary to make valid comparisons between fossil-fuel and nuclear plants. It is the purpose this work to study the chemical fractionation of the natural radionuclides in coal during combustion.

Experimental

Coal, bottom-ash, and electrostatic precipitator (ESP) fly-ash samples were obtained from two western coal-fired power plants. Plant A burns low-sulfur (0.52%), low-ash (9.2%) coal and Plant B burns low-sulfur (0.46%), high-ash (23.2%) coal. We also obtained from Plant B kilogram quantities of particle-sized stack fly ash. This stack fly ash was collected by a large cyclone separator mounted at the outlet of one of the ESP units.[5] Two separate sets of the four sized fractions were obtained. For each fraction as determined by centrifugal sedimentation, the mass median diameters (mmd) were 17, 6, 3.8, and 2.5 μm, Geometric standard deviations of the fractions were approximately 2.3, 2.1, 1.7, and 1.8 μm, respectively.

All samples were ground to 200 mesh when necessary, homogenized, packaged, and then counted for natural gamma radiation on an ultra-low background, Compton-suppression, gamma-ray spectrometer.

The ^{238}U natural radioactive-decay-chain series was found to be in secular equilbrium in the coal samples but not in the ash samples. During the combustion process a potential exists for decay-chain disequilibrium to occur, since many of the daughter radionuclides have quite different chemical and physical characteristics. Secondary post-fractionation radionuclides are those whose half-lives are long enough to produce gamma rays or gamma-ray-emitting daughters after secular equilibrium has been disrupted by the combustion process. The actual measured gamma ray may originate from a daughter further along the decay chain but prior to the next long-lived species.

The half-lives of these intermediary radionuclides are short enough so that secular equilibration can be assumed to have been reestablished for that section of the decay chain. The packaged samples were allowed to sit for 6 months. This provided the longest-lived intermediary radionuclide ^{234}Th (24.1 day) the opportunity to come to within 1% of secular equilibration with its parent ^{238}U.

Discussion

Enrichment factors relative to the input coal were calculated for the radionuclide contents observed. The enrichment factor (EF) is defined as the ratio of the concentration of a radionuclide (X) and ^{40}K in the sample, divided by the corresponding ration in the input coal.

$$EF = \frac{[X]\ \text{sample}/[^{40}K]\ \text{sample}}{[X]\ \text{coal}/[^{40}K]\ \text{coal}}$$

This effectively normalizes the apparent enrichment resulting from loss of carbon during the combustion process. Potassium-40 is used in this normalization calculation because its concentration remains constant in all samples; hence it was assumed to be a tracer for the alumino-silicate-dominated ash matrix.

Table 1 presents the EF value for the different samples from both plants. The ESP fly ash and bottom ash from both plants show no enrichment of the ^{232}Th-decay-chain daughters. This is expected since thorium and radium are essentially refractory elements and should remain with the ^{40}K in the ash matrix. Uranium behaves in quite

Table 1. Enrichment factor relative to input coal and normalized to ^{40}K[a]

Decay-chain origin	^{232}Th		^{238}U			^{235}U
Source after fractionation	^{228}Th	^{228}Ra	^{210}Pb	^{226}Ra	^{238}U	^{235}U
Plant A[b]						
ESP fly ash	0.89	0.90	0.48	1.02	0.71	0.70
Bottom ash	0.96	0.97	0.24	0.99	0.70	0.64
Plant B[c]						
ESP fly ash	0.96	0.98	0.74	1.02	0.94	0.85
Bottom ash	0.91	0.89	0.29	0.90	0.76	0.73
Scrubber ash	1.01	1.03	0.95	1.08	0.97	0.88

[a] ±10 to 20% propagated 1σ error from the mean.

[b] Samples from Plant A; input coal contains 11.3% H_2O, 9.2% ash, and 0.52% sulfur.

[c] Samples from Plant B; input coal contains 6.8% H_2O, 23.2% ash, and 0.46% sulfur.

a different manner. Both ^{235}U and ^{238}U show significant depletion in the fly ash from Plant A (low-ash coal) and the bottom ash from both Plants. The fly ash is not nearly as depleted in these uranium isotopes from Plant B (high-ash coal).

Lead-210 appears to be the most volatile radionuclide measured. It is quite depleted in the bottom ash from both plants and is less depleted in the fly ash from Plant B (high-ash coal). All EF values for the scrubber ash are close to unity. The wet scrubber is more efficient than the ESP for fly-ash removal (99.2% vs 97.%) and, therefore, retains more ash by weight than the ESP unit although it releases higher numbers of submicron particles to the atmosphere.[6] Since the wet scrubber is more efficient, its EF value might be expected to be near unity, and consequently any chemical enrichment in the submicron particulates would be obscured.

The ^{210}Pb depletion in the ESP bottom ash probably occurs as volatilization and later condensation onto the fly-ash matrix. Since heterogeneous condensation is a surface-area phenomenon, the lead would be expected to be enriched on the finer fly-ash particles. In Fig. 1, the stack (post ESP) sized fly ash shows a very strong increase in EF with decreasing particle size. This effect is consistent with the depletion of lead on the larger-sized ESP fly ash. Davison et al.[7] discuss this condensation mechanism more fully.

Assuming that secular equilibration exists between ^{210}Pb and ^{210}Po in the coal samples, the specific activity for both nuclides will be identical and therefore the total inventory of ^{210}Po for the coal combustion system can be estimated. Its post-combustion behavior was not studied in this work; but since polonium is more volatile than lead, it will probably condense onto the extremely small fly-ash particles after combustion. A study of the combustion chemistry and deposition properties of this important radionuclide is in progress.

Uranium's definite association with small particles has been previously observed.[8,9] It is slightly depleted in the bottom ash of both plants. Plant B (high-ash coal) has a fly-ash EF close to unity. However, this plant's sized stack fly ash shows a very definite EF increase with decreasing particle size (see Fig. 1). We propose a bimodal mechanism to explain this behavior. The coal contains uranium in two different phases, which affects its volatility upon combustion. Klein et al.[9] observed that uranium behaves in a manner intermediate between those elements remaining with the slag and those elements concentrating on the fly ash.

Breger[10] suggests that uranium enters the coal bed from ground water as the soluble uranyl dicarbonate $Na_2[UO_2(CO_3)_2]$ or sodium uranyl tricarbonate $Na_4[UO_2(CO_3)_3]$ complex. The slightly acidic environment of the coal decomposes this complex and the uranium quickly becomes absorbed by the coal with subsequent reduction to uraninite UO_2. If sufficient silica is present in solution, the mineral coffinite $U(SiO_4)_{1-x}(OH)_{4x}$ can form instead of uraninite. Since the uranium is in solution, it can migrate from cracks and joints into the coal matrix for some distance and can, therefore, be expected to reside in the coal in a very highly dispersed state. Uranium is enriched over thorium in these samples (Th/U = 2.0) compared to the average crustal ratio (Th/U = 4.0),[11] thus indicating the high mobility of uranium as compared to thorium during ground and surface water transport.

The characteristics of uranium during the combustion process depend upon the conditions of the furnace as well as its chemical and physical form in the input coal. Coal-fired power plants operate their burners with about a 10% stoichiometric excess of oxygen.[12] This should result in an oxidizing combustion environment with a temperature range of 1500 to 1600°C. Under these conditions, the volatile species UO_3 could be expected to form.[13,14] The possibility also exists for uranium to become incorporated into a silica melt during combustion if it were originally associated with a silicate (i.e., coffinite).

The existence of uranium bimodally in the coal can therefore give rise to both a volatile and nonvolatile species simultaneously, since both uraninite and coffinite can coexist in the pulverized and semihomogenized coal. The data in Table 1 support this relationship. The Plant B (high-ash coal) fly ash shows less uranium depletion than the Plant A (low-ash coal) fly ash. A higher percentage of the uranium is probably associated with the alumino-silicate minerals and is consequently available for incorporation into the silica-rich fly-ash matrix.

Thorium-228 could be slightly enriched in the stack fly ash when compared to INAA (Instrumental Neutron Activation Analysis) data for cerium, a nonenriched element

(see Fig. 1). Thorium (and to some extent uranium) is normally associated with the very chemically resistant mineral zircon $ZrSiO_4$,[15] which is a ubiquitous accessory mineral in many common rocks. Zircon does not weather easily and is commonly found in sedimentary environments. It is conceivable that the thorium observed in the coal system was deposited contemporaneously with the coal along with the other silicate-based minerals. These minerals make up the ash after the coal is burned. The small resistant mineral grains could be carried with the gases after combustion and follow the course of the fly ash. The thorium behavior in the sized fly ash could be explained if thorium existed in the coal as submicron particles.

The enrichment of ^{228}Ra and ^{226}Ra (see Fig. 1) is difficult to explain. Klein et al.[9] observes that barium (and hence probably radium) and thorium become incorporated into the fly-ash matrix. However, barium is known to form a volatile species $Ba(OH)_2$ in the presence of steam, and radium may also form a corresponding species. Figure 1 shows ^{226}Ra with a greater EF than ^{228}Ra. A portion of the ^{226}Ra will reside with the uraninite fraction of its ^{238}U parent as described earlier. This probably allows ^{226}Ra to form a more mobile species than the silicate bound ^{228}Ra (from the ^{232}Th chain) in a manner similar to the bimodally located uranium.

The behavior of the natural radioactive decay series throughout the coal deposition, combustion, and emission system can be described by the following:

- Associated with the accumulation of orgainic matter is a significant fraction of clay minerals, sand, and other inorganic sedimentary material. These materials contain the alumino-silicate minerals that will later comprise the coal fly ash and bottom ash. Herein is found the source of the ^{232}Th, ^{40}K, and a part of the silicate associated uranium.

- The organic accumulation environment ceases and a deposition environment prevails, which buries the organic matter. Coal metamorphism occurs.

- Ground and surface waters penetrate down through the overburden, invading the coal. These waters contain uranium as soluble uranyl carbonate salts and varying amounts of soluble silica.

- Uranium is absorbed by the coal and reduced to uraninite or coffinite, depending on the silica content of the water.

- Coal is mined, pulverized, and fed into the furnace for power production. Much of the alumino-silica minerals (mostly clay) form a melt and drop out as slag. Most of the thorium and radium isotopes follow. Lead-210 remains volatile and continues along with the gases and fly ash to the emission control system. Much of the uranium that is associated with the clays, or that which was mineralized as coffinite, also remain with the bottom ash. The uranium that is dispersed in the coal as uraninite becomes volatile as the UO_3 species and continues along with the gases, lead, and the fly ash.

- Somewhere down the flue line, first uranium and then lead preferentially condense out on the finer fly-ash particles because they have a high surface to mass ratio.

- The ESP collects most of the particulate mass. Those finer particles that bypass the ESP continue up the stack with the gases. They are very enriched in ^{210}Pb relative to the coal, and moderately enriched in ^{235}U and ^{238}U. Some slight enrichment is observed for ^{226}Ra (probably that associated with uraninite), ^{228}Ra, and ^{228}Th. The thorium is probably associated with fine zircon grains.

The degree to which each of the many possible mechanisms affect the final radionuclide concentrations cannot be ascertained from these data. The actual situation may be one mechanism, or more probably a combination of mechanisms. The mineralogical or chemical form in which the radionuclides or trace elements exist in the coal does have an important effect on their subsequent combustion chemistry and emission characteristics.

References

1. Eisenbud, Merril and Henry G. Petrow, Science 144, 228 (1964).
2. Martin, J.E., Harward, E.D., Oakley, D.T., Smith, J.M., and Bedrosian, P.H., in IAEA Symposium on Environmental Aspects of Nuclear Power Stations, New York, IAEA Conf. 700810-24 (1969) paper - IAEA-Sm-146/19, 325-337.
3. Hull, A.P., Nuclear News, 51-55, (April, 1974).
4. Moore, H.E., Martell, E.A., and Poet, S.E., Environ. Sci. Technol. 10, 586, (1976).
5. McFarland, A.R., Fisher, G.L., Prentice, B.A., and Bertch, R.W., Submitted for publication in Environ. Sci. Technol. (1976).
6. Ondov, J.M., Ragaini, R.C., and Biermann, A.H., presented at Amer. Chem. Soc. Meeting, Div. of Environ. Chem., Preprint UCRL-78050, 1976.
7. Davison, R.L., Natusch, D.F.S., and Wallace, J.R., Environ. Sci. Technol. 8, 1107 (1974).
8. Ragaini, R.C., Ondov, J.M., Proc. Int. Conf. Modern Trends in Activation Analysis, Munich, 1976, I, 654; Lawrence Livermore Laboratory, Preprint UCRL-77669.
9. Klein, D.H., Andren, A.W., Carter, J.A., Emery, J.F., Feldman, C., Fulkerson, W., Lyon, W.S., Ogle, J.C., Talmi, Y., Van Hook, R.I., and Bolton, N., Environ. Sci. Technol. 9, 973 (1975).
10. Breger, I.A., in IAEA Symposium on the Formation of Uranium Ore Deposits, Athens, IAEA-SM-183/29 (1974) pp. 99-124.
11. Mason, B., Principles of Geochemistry, 3rd. Ed., John Wiley & Sons (1966).
12. Babcock and Wilcox, Steam, Its Generation and Use, 38th Ed., Babcock and Wilcox, New York, 1972.
13. Rand, M.H., and Kubaschewski, O., The Thermochemical Properties of Uranium Compounds, Interscience (Wiley), New York, 1963.
14. Ackermann, R.J., Thorn, R.J., Alexander, C., and Tetenbaum, M., J. Phys. Chem. 64, 350 (1960).
15. Kirby, H.U., Mound Laboratory, Rept. MLM-2111 (1974).

NOTICE

"This report was prepared as an account of work sponsored by the United States Government. Neither the United States nor the United States Energy Research & Development Administration, nor any of their employees, nor any of their contractors, subcontractors, or their employees, makes any warranty, express or implied, or assumes any legal liability or responsibility for the accuracy, completeness or usefulness of any information, apparatus, product or process disclosed, or represents that its use would not infringe privately-owned rights."

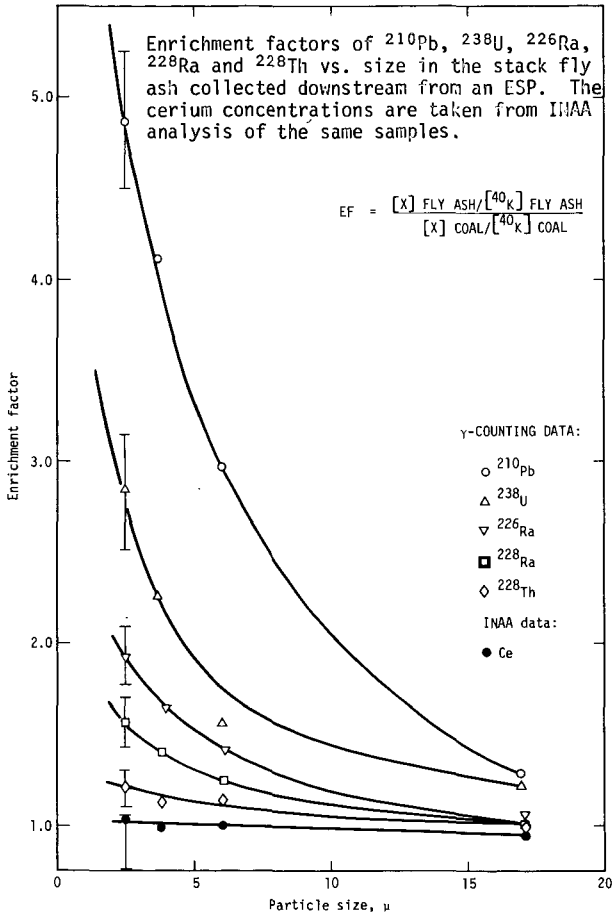
Enrichment factors of ^{210}Pb, ^{238}U, ^{226}Ra, ^{228}Ra and ^{228}Th vs. size in the stack fly ash collected downstream from an ESP. The cerium concentrations are taken from INAA analysis of the same samples.
$EF = \frac{[X]\ FLY\ ASH/[^{40}K]\ FLY\ ASH}{[X]\ COAL/[^{40}K]\ COAL}$
γ-COUNTING DATA:
^{210}Pb
^{238}U
^{226}Ra
^{228}Ra
^{228}Th
INAA data:
Ce
Enrichment factor
5.0
4.0
3.0
2.0
1.0
0
5
10
15
20
Particle size, μ